Role of Absorption on the Generation of Quantum-Correlated Photon Pairs Through FWM

Nuno A. Silva and Armando Nolasco Pinto, *Senior Member, IEEE*

***Abstract*— The impact of fiber absorption on the generation rate of quantum-correlated photon pairs through spontaneous four-wave mixing in optical fibers is studied theoretically. We quantify the impact of the loss through the analysis of the Cauchy–Schwarz correlation parameter and the Clauser, Horne, Shimony, and Holt inequality. Results show that fiber loss can improve the quantum-correlation between the photon pairs. This is a consequence of the decrease of the individual signal and idler photon-fluxes, which reduces the rate of uncorrelated photons generated through Raman scattering inside the optical fiber. Findings show that a high degree of polarization entanglement is obtained when the ratio of signal to idler photon-fluxes lies between 0.5 and 0.8, in a regime with high losses on the signal wave.**

***Index Terms*— Nonlinear optics, nonlinearities, optical mixing, Raman scattering.**

I. Introduction

QUANTUM-CORRELATED photon pairs are essential for quantum technologies, such as quantum information [1]. In this context, the generation of correlated photon pairs inside optical waveguides appears as important topic for quantum key distribution [1]. The four-wave mixing (FWM) process provides an efficient method of generating correlated photon pairs already inside a waveguide. Those photons, obtained through FWM, has been used mainly in quantum key distribution experiments, through the implementation of heralded single photon sources [2] and entangled photon sources [3], [4].

Efficient generation of quantum-correlated photon pairs through spontaneous FWM demands perfect phase-matching condition and waveguides with high value of nonlinear coefficient [5]–[7]. Recent developments of photonic crystal fibers (PCF) and chalcogenide glass waveguides have enable to produce optical waveguides with high nonlinear coefficient and a near-zero dispersion wavelength [8], [9]. Waveguides with high nonlinear coefficient can be used for efficient generation of photon pairs over short distances [10], [11]. This is essential to implement integrated on-chip quantum technologies [12]. However, waveguides with high nonlinear coefficient usually presents high values of loss [8]–[10]. A complete description of the generation of quantum-correlated photon pairs through spontaneous FWM in loss waveguides remains an open issue, to the best of our knowledge.

The spontaneous FWM in optical fibers as a source of photon pairs was investigated experimentally in [13], [14] in the single-pump configuration. In [15] authors report the generation of correlated photon pairs by means of a reversed degenerate FWM process. Recently, in [16] authors investigate the generation of identical photons using a dual-pump counter-propagating scheme. Subsequent studies have used the FWM process to implement polarization [11], [17]–[20], time-bin [21], [22], and frequency [23] entangled photon pair sources. The generation of quantum-correlated photon pairs was already studied experimentally in chalcogenide glass waveguides, see for instance [8], [10], [24].

The spontaneous FWM was also studied theoretically in [25], and their work was latter extend to include the pump pulsed regime [26], [27], and to include the impact of the spontaneous Raman scattering that occurs inside the fiber [28]–[31]. A vectorial theory of the combined processes of FWM and Raman scattering was presented in [6], considering various pumping configurations. In [30], authors present a quantum theory of phase-sensitive parametric amplifier in $\chi^{(3)}$ materials, including the effect of linear loss. Recently, in [32] authors investigated the generation of correlated photon pairs through FWM using silicon waveguides, in the presence of three different sources of losses.

The aim of this paper is to give a complete description of the generation of photon-pairs through the combined processes of FWM and Raman scattering in a medium with non-negligible loss, $\alpha(\omega)L \gg 1$. In this paper we expand previous studies related with the generation of quantum-correlated photon pairs in order to include the waveguide absorption [6], [28], [31]. The obtained results can help to guide the implementation of on-chip quantum technologies.

This paper contains six sections. In section II, we present the formalism of the evolution of the optical field operator in a medium with non-negligible loss. In section III, we apply that formalism to the co-polarized spontaneous FWM process in the single-pump configuration. Section IV, describes the impact of the waveguide absorption on the photon-flux and on the second-order coherence function. In section V, we discuss the influence of waveguide loss on the Cauchy-Schwarz correlation parameter and on the Clauser, Horne, Shimony, and Holt (CHSH) inequality. The main results of this paper are summarized in section VI.

Manuscript received March 8, 2012; revised August 1, 2012; accepted August 9, 2012. Date of publication August 17, 2012; date of current version August 29, 2012. This work was supported in part by the Fundação para a Ciência e Tecnologia (FCT), through the Ph.D. program under Grant SFRH/BD/63958/2009, the FCT and European Union Fundo Europeu de Desenvolvimento Regional (FEDER) through Project PTDC/EEA-TEL/103402/2008 (QuantPriv-Tel), and the FCT and the Instituto de Telecomunicações, under the PEst-OE/EEI/LA0008/2011 Program, Project "P-Quantum."

The authors are with the Department of Electronics, Telecommunications and Informatics, University of Aveiro and Instituto de Telecomunicações, Aveiro 3810-193, Portugal (e-mail: nasilva@av.it.pt; anp@ua.pt).

Color versions of one or more of the figures in this paper are available online at http://ieeexplore.ieee.org.

Digital Object Identifier 10.1109/JQE.2012.2213802

II. Theoretical Model

In this section, we present the equation of motion of the optical field annihilation operator inside an optical fiber, for each of the polarization modes $j = x$ or y. Under the rotating-wave approximation, the quantum version of the nonlinear Schrödinger equation in optical fibers in the frequency domain is given by [6], [30], [33]–[36]

$$\frac{\partial \hat{A}_j(z,\omega)}{\partial z} = i\sum_k \tilde{R}^{(1)}_{jk}(\omega)\hat{A}_k(z,\omega) + \frac{i\hbar\omega_0}{(2\pi)^2}\sum_{klm}\iint d\omega_1 d\omega_2 \times \tilde{R}^{(3)}_{jklm}(\omega_2-\omega_1)\hat{A}^\dagger_l(z,\omega_1)\hat{A}_m(z,\omega_2)\hat{A}_k(z,\omega+\omega_1-\omega_2) + \frac{i\sqrt{\hbar\omega_0}}{2\pi}\sum_k\int d\omega_1 \hat{m}_{jk}(z,\omega-\omega_1)\hat{A}_k(z,\omega_1)+\hat{l}_j(z,\omega), \quad (1)$$

where $j,k,l,m = x$ or y, ω_0 is the carrier frequency of the electromagnetic field, $\hat{A}_j(z,\omega)$ is the slowly varying field annihilation operator in the frequency domain, which satisfies the commutation relation

$$\left[\hat{A}_j(z,\omega), \hat{A}^\dagger_k(z,\omega')\right] = 2\pi\delta_{jk}\delta(\omega-\omega'), \quad (2)$$

$\tilde{R}^{(1)}_{jk}(\omega)$ is the Fourier transform of $R^{(1)}_{jk}(\tau)$, and represents the linear response function of the fiber, given by sec. 2.1 of [5], and [37]

$$\tilde{R}^{(1)}_{jk}(\omega) = \beta_j(\omega) + \frac{i}{2}\alpha_j(\omega) - \frac{\omega}{2}\mathbf{B}_{jk}, \quad (3)$$

which includes both dispersion $\beta_j(\omega)$ and birefringence $\mathbf{B}_{jk}$ properties of the fiber, as well the fiber losses $\alpha_j(\omega)$, see for instance sec. 1.2 of [5], and [38]. In (1), $\tilde{R}^{(3)}_{jklm}(\Omega)$ is the third-order nonlinear response function of the optical fiber, given by [6], [39]–[41]

$$\tilde{R}^{(3)}_{jklm}(\Omega) = \gamma\frac{1-f_R}{3}\left(\delta_{jk}\delta_{lm}+\delta_{jl}\delta_{km}+\delta_{jm}\delta_{kl}\right) + \gamma f_R\tilde{R}_a(\Omega)\delta_{jk}\delta_{lm} + \gamma\frac{f_R}{2}\tilde{R}_b(\Omega)\left(\delta_{jl}\delta_{km}+\delta_{jm}\delta_{kl}\right), \quad (4)$$

and governs the nonlinear processes that occurs inside the fiber such as FWM and Raman scattering. In (4), Ω is the Stokes ($\Omega < 0$) or anti-Stokes ($\Omega > 0$) frequency shift, γ is the nonlinear coefficient of the fiber, $f_R = 0.18$ [42] is the fractional contribution of the Raman process to the nonlinear refractive index, $\tilde{R}_a(\Omega)$ and $\tilde{R}_b(\Omega)$ are the isotropic and anisotropic Raman response, respectively, in the frequency domain [43]. The co-polarized and orthogonal Raman gain is obtained from (4), and are given by $g_{Rx}(\Omega) = 2\,\mathrm{Im}[\tilde{R}^{(3)}_{xxxx}(|\Omega|)]$, and $g_{Ry}(\Omega) = 2\,\mathrm{Im}[\tilde{R}^{(3)}_{xyxy}(|\Omega|)]$ [6], [39]–[41]. In (1), $\hat{m}_{jk}(z,\Omega)$ is the noise operator due to the presence of a phonon reservoir, and $\hat{l}_j(z,\omega)$ represents the photon absorption reservoir. The $\hat{m}_{jk}(z,\Omega)$ noise operator accounts for the spontaneous Raman scattering process in optical fibers. The Raman noise operator is modeled as a collection of localized and independent harmonic oscillators with spectral weight proportional to the imaginary part of the third-order nonlinear response of the fiber. Moreover, it is assumed that the initial state of the phonons is in thermal equilibrium, with occupation number following the Boltzman distribution [30], [33]–[35]. The $\hat{l}_j(z,\omega)$ operator describes the noise introduce by the fiber loss mechanism, through the coupling of the optical field with a thermal photon reservoir with a population following the Boltzman distribution, and spectral weight proportional to the fiber loss coefficient [30], [32]–[34]. The noise operators satisfy the commutation relations [6], [30], [34]

$$\left[\hat{m}_{jk}(z,\Omega), \hat{m}^\dagger_{lm}(z',\Omega')\right] = 2\pi\delta(z-z')\delta(\Omega-\Omega') \times 2\,\mathrm{Im}\left[\tilde{R}^{(3)}_{jklm}(\Omega)\right], \quad (5)$$

and

$$\left[\hat{l}_j(z,\omega), \hat{l}^\dagger_k(z',\omega')\right] = 2\pi\delta_{jk}\delta(z-z')\delta(\omega-\omega')\alpha_j(\omega). \quad (6)$$

The expectation values for the reservoirs are given by

$$\langle\hat{m}^\dagger_{jk}(z,\Omega)\hat{m}_{lm}(z',\Omega')\rangle = 2\pi\delta(z-z')\delta(\Omega-\Omega') \times 2\,\mathrm{Im}\left[\tilde{R}^{(3)}_{jklm}(|\Omega|)\right](\mathcal{N}_{th}+\Theta(-\Omega)), \quad (7)$$

$$\langle\hat{l}^\dagger_j(z,\omega)\hat{l}_k(z',\omega')\rangle = 2\pi\delta_{jk}\delta(z-z')\delta(\omega-\omega') \times\alpha_j(\omega)\mathcal{N}_{th}, \quad (8)$$

where $\mathcal{N}_{th} = [\exp\{\hbar|\Omega|/(k_BT)-1\}]^{-1}$, k_B is the Boltzmann's constant, T is the temperature, and $\Theta(-\Omega)$ is the Heaviside step function.

In the following sections, we will use the formalism presented in (1)-(8), in order to quantify the impact of fiber absorption on the generation of quantum-correlated photon pairs through spontaneous FWM process.

III. Single-Pump FWM Configuration

In the single-pump configuration, the FWM process can be decomposed in two different polarization schemes, co-polarized and orthogonal. In the co-polarized the signal and idler photons are generated parallel to the pump field, whereas in the orthogonal they are generated perpendicular to the pump [6], [40]. In this work, we focus only on the co-polarized scheme.

We assume that, the fiber length is much shorter than the walk-off length. In that regime, we can apply the quasi-continuous wave approximation, described in sec. 7.4 of [5]. Moreover, we consider that the pump field is much more intense than the signal and idler waves, and remains undepleted, see for instance sec. 10.2 of [5]. Hence, the pump field can be treated classically, ignoring the pump quantum fluctuations [30]. Separating (1) into the frequency components, the evolution of the pump, signal and idler waves inside the fiber can be written as [30]

$$\bar{A}_p(z) = \bar{A}_p(0)\exp\left\{\left(i\beta_p z+\gamma P_x(0)z_e\right)-\frac{\alpha_p}{2}z\right\}, \quad (9a)$$

$$\frac{\partial\hat{A}_u(z)}{\partial z} = i\left(\beta_u+\frac{i}{2}\alpha_u+\gamma\xi(\Omega_{up})P_x(z)\right)\hat{A}_u(z) + i\gamma\eta(\Omega_{up})\bar{A}^2_p(z)\hat{A}^\dagger_v(z) + i\hat{m}(z,\Omega_{up})\bar{A}_p(z) + \hat{l}(z,\omega_u), \quad (9b)$$

where $\hat{A}_u(z) \equiv \hat{A}_x(z,\omega_u)$, $\beta_u \equiv \beta_x(\omega_u)$, $\hat{m}(z,\Omega) \equiv \hat{m}_{xx}(z,\Omega)$, $\hat{l}(z,\omega_u) \equiv \hat{l}_x(z,\omega_u)$, and $\alpha_u \equiv \alpha_x(\omega_u)$. In (9b) $u \neq v = s$ or i and represent the signal and idler fields, and $\Omega_{up} = \omega_u - \omega_p$. $\bar{A}_p(z)$ is such that $P_x(z) = |\bar{A}_p(z)|^2$ is the

pump power, z_e is the effective length of the fiber at pump frequency at a given distance z, given by sec. 4.1 of [5]

$$z_e = \frac{1 - e^{-\alpha_p z}}{\alpha_p}. \tag{10}$$

In (9b), $\xi(\Omega_{up})$ and $\eta(\Omega_{up})$ are given by [6], [40]

$$\xi(\Omega_{up}) = 2 - f_R + f_R\left(\tilde{R}_a(\Omega_{up}) + \tilde{R}_b(\Omega_{up})\right), \tag{11a}$$

$$\eta(\Omega_{up}) = 1 - f_R + f_R\left(\tilde{R}_a(\Omega_{up}) + \tilde{R}_b(\Omega_{up})\right), \tag{11b}$$

In the most general case, when the pump power loss is taken into account, equation (9b) only have a power series solution [30]. In that case, after some mathematical manipulation, the evolution of the signal and idler annihilation operators at a given distance L in the fiber are given by

$$\hat{A}_u(L) = \mu_u(L,0)\hat{A}_u(0) + \nu_u(L,0)\hat{A}_v^{\dagger}(0) + \hat{N}(L,\omega_u) + \int_0^L dz\left(\hat{l}(z,\omega_u)\mu_u(L,z) + \hat{l}^{\dagger}(z,\omega_v)\nu_u(L,z)\right), \tag{12}$$

where

$$\hat{N}(L,\omega_u) = i\int_0^L \hat{m}(z,\Omega_{up})\Big(\bar{A}_p(z)\mu_u(L,z) - \bar{A}_p^*(z)\nu_u(L,z)\Big)dz. \tag{13}$$

In (12) and (13)

$$\mu_s(L,z) = e^{p(L,z,\omega_s)}\sum_{n=0} s_n(z)L_e^n(z), \tag{14a}$$

with $s_0 = 1$ and $a_0^* = 0$,

$$\nu_s(L,z) = e^{p(L,z,\omega_s)}\sum_{n=0} s_n(z)L_e^n(z), \tag{14b}$$

with $s_0 = 0$ and $a_0^* = 1$,

$$\mu_i(L,z) = e^{p(L,z,\omega_i)}\sum_{n=0} a_n(z)L_e^n(z), \tag{14c}$$

with $s_0 = 0$ and $a_0^* = 1$,

$$\nu_i(L,z) = e^{p(L,z,\omega_i)}\sum_{n=0} a_n(z)L_e^n(z), \tag{14d}$$

with and $s_0 = 1$ and $a_0^* = 0$.

In (14), $L_e(z) = (1 - \exp\{-\alpha_p(L-z)\})/\alpha_p$, and

$$p(L,z,\omega_u) = -\frac{\alpha_s + \alpha_i + 2i\,\Delta\beta}{4}(L-z) + i\left(\beta_u(L-z) + \gamma\, P_x(0)L_e(z)\right), \tag{15}$$

where $\Delta\beta$ is the phase-matching condition, given by [40]

$$\Delta\beta = \beta_3(\omega_p - \omega_0)(\omega_p - \omega_s)^2, \tag{16}$$

where β_3 is the third-order dispersion coefficient at zero-dispersion frequency, ω_0. In (14), the coefficients s_1 and a_1 are given by

$$s_1(z) = i\gamma\, P_x(z)\left(\xi(\Omega_{sp}) - 1\right)s_0 + i\gamma\,\eta(\Omega_{sp})\bar{A}_p^2(z)a_0^* - \frac{\alpha_s + \alpha_i + 2i\,\Delta\beta}{4}s_0, \tag{17a}$$

$$a_1^*(z) = -i\gamma\, P_x(z)\left(\xi^*(\Omega_{ip}) - 1\right)a_0^* - i\gamma\,\eta^*(\Omega_{ip})\bar{A}_p^{2*}(z)s_0 + \frac{\alpha_s + \alpha_i + 2i\,\Delta\beta}{4}a_0^*. \tag{17b}$$

For $n \geq 1$ the coefficients s_{n+1} and a_{n+1} are given by

$$s_{n+1}(z) = \frac{n}{n+1}\alpha_p s_n(z) - \frac{\alpha_s + \alpha_i + 2i\,\Delta\beta}{4(n+1)}s_n(z) + i\frac{\gamma\, P_x(z)}{n+1}\left(\xi(\Omega_{sp}) - 1\right)\left(s_n(z) - \alpha_p s_{n-1}(z)\right) + i\frac{\gamma\,\eta(\Omega_{sp})}{n+1}\bar{A}_p^2(z)\left(a_n^*(z) - \alpha_p a_{n-1}^*(z)\right), \tag{18a}$$

$$a_{n+1}^*(z) = \frac{n}{n+1}\alpha_p a_n^*(z) + \frac{\alpha_s + \alpha_i + 2i\,\Delta\beta}{4(n+1)}a_n^*(z) - i\frac{\gamma\, P_x(z)}{n+1}\left(\xi^*(\Omega_{ip}) - 1\right)\left(a_n^*(z) - \alpha_p a_{n-1}^*(z)\right) - i\frac{\gamma\,\eta^*(\Omega_{ip})}{n+1}\bar{A}_p^{2*}(z)\left(s_n(z) - \alpha_p s_{n-1}(z)\right). \tag{18b}$$

In the case of orthogonal FWM polarization scheme, where the pump evolves on the x fiber axis and the signal-idler photons are created on the y axis, it is necessary to change some parameters on the theoretical model present in (9)-(18). The loss and dispersion coefficients for the signal and idler waves should be replaced by $\alpha_x(\omega_u) \equiv \alpha_y(\omega_u)$, and $\beta_x(\omega_u) \equiv \beta_y(\omega_u)$, respectively. In this polarization scheme, the phase matching condition is given by [40]

$$\Delta\beta_y = 2\frac{\omega_p}{c}\delta n + \Delta\beta, \tag{19}$$

where δn is the refractive-index difference between the fiber two axis, and $\Delta\beta$ is given by (16). Moreover, for the orthogonal polarization scheme $\xi(\Omega_{up})$ and $\eta(\Omega_{up})$ should be replaced by [6]

$$\xi_y(\Omega_{up}) = 2(1 - f_R)/3 + f_R\left(\tilde{R}_a(0) + \tilde{R}_b(\Omega_{up})/2\right), \tag{20a}$$

$$\eta_y(\Omega_{up}) = (1 - f_R)/3 + f_R\tilde{R}_b(\Omega_{up})/2. \tag{20b}$$

IV. Photon-Flux and the Second-Order Coherence Function

In this section, we focus on the impact of the fiber absorption on the photon-flux generated through spontaneous FWM process. We also examine the statistics of the individual signal and idler frequency modes in a loss media in terms of the second-order coherence function, $g_u^{(2)}(0)$.

The photon-flux for the signal and idler fields is given by [6]

$$\mathcal{I}_u(L,\tau) = \langle\hat{B}_u^{\dagger}(L,\tau)\hat{B}_u(L,\tau)\rangle = \frac{1}{(2\pi)^2}\iint d\omega_u d\omega_{u'}e^{i(\omega_u - \omega_{u'})\tau} \times H_u^*(\omega_u)H_u(\omega_{u'})\mathcal{F}_u(L), \tag{21}$$

where $\mathcal{F}_u(L) = \langle\hat{A}^{\dagger}(L,\omega_u)\hat{A}(L,\omega_{u'})\rangle$ is the photon-flux spectral density, $H_u(\omega_u)$ is a filter function centered at $\bar{\omega}_u$. For the signal field the filter central frequency is $\bar{\omega}_s$, whereas for the idler is $\bar{\omega}_i$, such that $2\omega_p = \bar{\omega}_s + \bar{\omega}_i$. For a filter bandwidth much smaller than its mid-frequency, $\Delta\omega_u = 2\pi\,\Delta\nu_u \ll \bar{\omega}_u$ [44], and according with (7), (8) and (12) the photon-flux can be written as

$$\mathcal{I}_u(L,\tau) \approx \Delta\nu_u\,\mathcal{F}_{\bar{u}}(L). \tag{22}$$

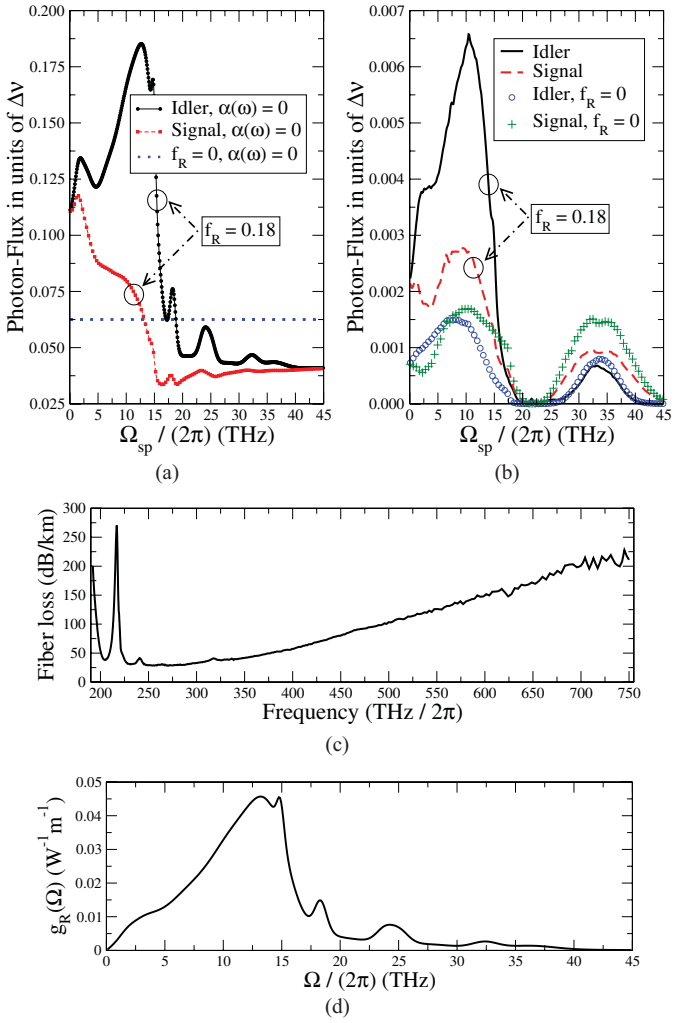

Fig. 1. (a) and (b) Idler and signal photon-flux per unit of filter bandwidth, $\Delta\nu$, as a function of the frequency separation between pump and signal fields. In both plots when $f_R = 0$ the photons are generated only by the FWM process. (c) Fiber loss spectrum [9]. In (a), we do not consider the fiber loss, $\alpha(\omega) = 0$, whereas in (b) fiber loss present in (c) is taken into account. (d) Raman gain coefficient [42]. (a) Without absorption. (b) With absorption. (c) Fiber loss spectrum. (d) Raman gain coefficient.

In (22) $\Delta\nu_u = 1/(2\pi)\int d\omega_u |H_u(\omega_u)|^2$, and the photon-flux spectral density $\mathcal{F}_u(L)$ is calculated at frequency $\bar{\omega}_u$

$$\begin{aligned}\mathcal{F}_{\bar{u}}(L) &= \langle \hat{A}^{\dagger}(L,\bar{\omega}_u)\hat{A}(L,\bar{\omega}_u)\rangle \\ &= |\nu_{\bar{u}}(L,0)|^2 + \alpha_{\bar{u}}\mathcal{N}_{\bar{u}}\int_0^L dz|\mu_{\bar{u}}(L,z)|^2 \\ &\quad + \alpha_{\bar{v}}(\mathcal{N}_{\bar{v}}+1)\int_0^L dz|\nu_{\bar{u}}(L,z)|^2 \\ &\quad + (\mathcal{N}_{\bar{u}p}+\Theta_{\bar{u}p})g_R(\bar{\Omega}_{up}) \\ &\quad \times \int_0^L dz\left|\bar{A}_p(z)\mu_{\bar{u}}(L,z) - \bar{A}_p^*(z)\nu_{\bar{u}}(L,z)\right|^2, \quad (23)\end{aligned}$$

where $\bar{u} \equiv \bar{\omega}_u$, $\Theta_{\bar{u}p} \equiv \Theta(-\bar{\Omega}_{up})$, $\bar{\Omega}_{up} = \bar{\omega}_u - \omega_p$, $\mathcal{N}_{\bar{u}} \equiv [\exp\{\hbar|\bar{\omega}_u|/(k_BT) - 1\}]^{-1}$, and $\mathcal{N}_{\bar{u}p} \equiv [\exp\{\hbar|\bar{\Omega}_{up}|/(k_BT) - 1\}]^{-1}$.

In Fig. 1, we present the photon-flux, given by (22), as a function of frequency detuning between pump and signal fields, Fig. 1(a) and Fig. 1(b). In the figure it is also presented the fiber loss spectrum, Fig. 1(c), and the Raman gain coefficient, Fig. 1(d). The silica based high nonlinear photonic crystal fiber parameters are $\gamma = 95\ \mathrm{W^{-1}km^{-1}}$, zero-dispersion wavelength $\lambda_0 = \lambda_p = 1257.45$ nm, $\beta_3 = -0.356\ \mathrm{ps^3/km}$, $\alpha_p = 37.2$ dB/km [9], [45], $\Delta\beta = 0$, $T = 300$ K, length $L = 600 > 1/\alpha_p$ m, and $P_x(0) = 22.7$ mW such that $\gamma P_x(0) z_e = 0.25$. When $\alpha(\omega) = 0$ we obtain $P_x(0) = 4.4$ mW due to the fact that $z_e = L$. These values were obtained from the fiber manufacturer. We use this fiber in order to be able to operate in the $\alpha(\omega)L \gg 1$ regime. The fiber Raman response function, $\tilde{R}_a(\Omega_{up}) + \tilde{R}_b(\Omega_{up})$, was taken from [42], and the fiber loss spectrum was obtained from NKT Photonics [9]. Moreover, we assume an identical rectangular shape for both signal and idler optical filters.

Figure 1(a) and Fig. 1(b) show the signal and idler photon-fluxes, given by (22), as a function of frequency detuning between pump and signal fields. In Fig. 1(a), we do not consider the fiber loss, $\alpha(\omega) = 0$ in (22), whereas in Fig. 1(b), the fiber loss spectrum present in Fig. 1(c) is taken into account. In both figures, Fig. 1(a) and Fig. 1(b), when $f_R = 0$ the Raman scattering process is ignored. It can be seen in Fig. 1(a) and in Fig. 1(b), that the wavelength dependence of the fiber loss coefficient changes significantly the spectrum of both signal and idler photon-fluxes. Results also show that the fiber loss reduces the photon-flux due to the fiber absorption of the signal and idler photons, and due to the fact that the pump field, given by (9a), is attenuated during the propagation on the fiber. When $20 < \Omega_{sp}/(2\pi) < 25$ (THz) the photon-flux for signal and idler fields is almost null. This is due to the fact that, the idler frequency corresponds to the peak on the spectrum of the fiber loss presented on Fig. 1(c). According with (23) the signal photon-flux is proportional to the idler absorption coefficient. Since $\alpha_{\bar{i}} \approx 300$ dB/km this leads to an almost null photon-flux for the signal wave. This mean that, the number of photons generated in the signal field depends on the fiber absorption coefficient on the idler wave. The opposite is also true (23).

The statistics of the individual signal and idler frequency modes in a loss medium can be assessed through the analysis of the second-order coherence function defined as [46], [47]

$$g_u^{(2)}(0) = \frac{\int_{t_0}^{t_0+T_0}\int \langle :I_u(L,t)I_u(L,t'):\rangle dt\,dt'}{\int_{t_0}^{t_0+T_0}\int \mathcal{I}_u(L,t)\mathcal{I}_u(L,t')dt\,dt'}, \quad (24)$$

where $I_u(L,\tau) = \hat{B}_u^{\dagger}(L,t)\hat{B}_u(L,t)$, :: denotes operator normal ordering, and T_0 is the time detection window. Using (12), (21), and (22)

$$\begin{aligned}\langle :I_u(L,t)I_u(L,t'):\rangle &= \left|\langle \hat{B}_u^{\dagger}(L,t')\hat{B}_u(L,t)\rangle\right|^2 \\ &\quad + \mathcal{I}_u(L,t)\mathcal{I}_u(L,t') \\ &= \left|\phi_u(t,t')\right|^2|\mathcal{F}_{\bar{u}}(L)|^2 + (\Delta\nu_u\mathcal{F}_{\bar{u}}(L))^2, \quad (25)\end{aligned}$$

which represents the self-correlation amplitude for the signal or idler waves. In (25), $\mathcal{F}_{\bar{u}}(L)$ is given by (23) and

$$\phi_u(t,t') = \frac{1}{2\pi}\iint d\omega_u d\omega_{u'} H_u^*(\omega_u)H_u(\omega_{u'})e^{i(\omega_u t' - \omega_{u'}t)}. \quad (26)$$

Finally, the second-order coherence function is given by

$$g_{\bar{u}}^{(2)}(0) = 1 + \frac{\iint |H_u(\omega_u)|^2 |H_u(\omega_{u'})|^2 \left(\frac{2-2\cos\left(T_0(\omega_u-\omega_{u'})\right)}{(\omega_u-\omega_{u'})^2}\right) d\omega_u d\omega_{u'}}{(\Delta\omega_u T_0)^2}. \quad (27)$$

From (27) we can see that, the absorption reservoir does not change the statistics of the signal or idler fields. However, depending of the value of $\Delta\omega_u T_0$ we obtain different statistical regimes for the signal and idler fields. If $\Delta\omega_u T_0 \ll 1$ we obtain $g_{\bar{u}}^{(2)}(0) = 2$, which represents a thermal statistics. However, if $\Delta\omega_u T_0 \gg 1$ we obtain $g_{\bar{u}}^{(2)}(0) = 1$, a Poissonian distribution. For all the other values of $\Delta\omega_u T_0$ the second-order coherence function varies between $1 < g_{\bar{u}}^{(2)}(0) < 2$, which represents a multithermal statistics. This is in-line with previous reported experimental works, see for instance [48], [49].

V. Two-Photon Correlation

In this section, we analyze the impact of fiber absorption on the generation of quantum-correlated photon pairs through spontaneous FWM in optical fibers. We analyze the degree of quantum correlation in terms of the Cauchy-Schwarz inequality, and the degree of polarization entanglement in terms of the CHSH inequality. A violation of the Cauchy-Schwarz inequality, given by (28), determines the nonclassical nature of the photons, whereas a violation of the CHSH inequality, given by (34), represents the nonlocality of light [50], [51].

The Cauchy-Schwarz inequality can be written as [50], [52]

$$\mathcal{G}^{CS}(\tau) = \frac{G_{(si)}^{(2)}(\tau)}{\sqrt{G_s^{(2)}(\tau)\, G_i^{(2)}(\tau)}} \leq 1, \quad (28)$$

where the nonclassical regime is obtained when $\mathcal{G}^{CS}(\tau) > 1$. This mean that, the photons of different modes have a higher correlation than the photons of the same mode. A larger value of $\mathcal{G}^{CS}(\tau)$ corresponds to a larger degree of nonclassical correlation. In (28), $G_{(si)}^{(2)}(\tau)$ is the cross-correlation between signal and idler frequency modes, given by

$$\begin{aligned} G_{(si)}^{(2)}(\tau) &= \langle \hat{B}_i^\dagger(L,t)\hat{B}_s^\dagger(L,t+\tau)\hat{B}_s(L,t+\tau)\hat{B}_i(L,t)\rangle \\ &= \left|\langle \hat{B}_s(L,t+\tau)\hat{B}_i(L,t)\rangle\right|^2 + \mathcal{I}_i(L,t)\mathcal{I}_s(L,t+\tau), \end{aligned} \quad (29)$$

where, according with (7), (8) and (12)

$$\left|\langle \hat{B}_s(L,t+\tau)\hat{B}_i(L,t)\rangle\right|^2 = |\phi_c(\tau)|^2 \left|\mathcal{F}^c(L,\bar{\omega}_s,\bar{\omega}_i)\right|^2. \quad (30)$$

In (30), $\phi_c(\tau)$ is given by

$$\phi_c(\tau) = \frac{1}{2\pi}\int d\omega H_s(\omega-\bar{\omega}_s) H_i(\bar{\omega}_s-\omega) e^{-i\omega\tau}, \quad (31)$$

and

$$\begin{aligned} \mathcal{F}^c(L,\bar{\omega}_s,\bar{\omega}_i) &= \langle \hat{A}(L,\bar{\omega}_s)\hat{A}(L,\bar{\omega}_i)\rangle \\ &= \mu_{\bar{s}}(L,0)\nu_{\bar{i}}(L,0) + \alpha_{\bar{s}}(\mathcal{N}_{\bar{s}}+1)\int_0^L dz \mu_{\bar{s}}(L,z)\nu_{\bar{i}}(L,z) \\ &\quad + \alpha_{\bar{i}}\mathcal{N}_{\bar{i}}\int_0^L dz \nu_{\bar{s}}(L,z)\mu_{\bar{i}}(L,z) - (\mathcal{N}_{\bar{i}p}+\Theta_{\bar{i}p}) g_R(\bar{\Omega}_{ip}) \\ &\quad \times \int_0^L \left(\bar{A}_p(z)\mu_{\bar{s}}(L,z) - \bar{A}_p^*(z)\nu_{\bar{s}}(L,z)\right) \\ &\quad \times \left(\bar{A}_p(z)\mu_{\bar{i}}(L,z) - \bar{A}_p^*(z)\nu_{\bar{i}}(L,z)\right) dz. \end{aligned} \quad (32)$$

The $G_u^{(2)}(\tau)$ coefficient is the self-correlation amplitude, and it is given by (25), with $t' = t+\tau$. From (22), (31) and (32) we can evaluate the true and the accidental coincidences counting rates, given respectively by [6]

$$R_{\text{pair}} = \int_0^{\tau_c} |\phi_c(\tau)|^2 |\mathcal{F}^c(L,\bar{\omega}_s,\bar{\omega}_i)|^2 d\tau, \quad (33a)$$

$$R_{\text{acc}} = \int_0^{\tau_c} (\Delta\nu)^2 \mathcal{F}_{\bar{s}}(L)\mathcal{F}_{\bar{i}}(L) d\tau, \quad (33b)$$

where τ_c is the coincidence time window.

Figure 2 shows the Cauchy-Schwarz correlation parameter, $\mathcal{G}^{CS}(0)$, given by (28), as a function of the frequency detuning between pump and signal, Fig. 2(a), and as a function of fiber length, Fig. 2(b). It can be seen in Fig. 2(a) that the fiber loss increases the degree of nonclassical correlation between signal and idler photons. Nevertheless, the presence of the Raman scattering process tends to degrade the photon pair correlation, since the Raman scattering process generates uncorrelated signal and idler photons. This degradation can be seen in Fig. 2(a) where $\mathcal{G}^{CS}(0)$ tends to take a high value when $f_R = 0$. When $20 < \Omega_{sp}/(2\pi) < 25$ (THz) the $\mathcal{G}^{CS}(0)$ parameter reaches its maximum value, which corresponds to the minimum of the signal and idler photon-fluxes, see Fig. 1(b). That maximum on the $\mathcal{G}^{CS}(0)$ parameter is due to the decrease on the accidental coincidences, given by $\mathcal{I}_i(L,t)\mathcal{I}_s(L,t+\tau)$ in (29). That term is almost null when $20 < \Omega_{sp}/(2\pi) < 25$ (THz), due to the fact that $\alpha_{\bar{i}}$ reaches its maximum value.

It can be seen in Fig. 2(b) that the $\mathcal{G}^{CS}(0)$ parameter increases with the increase of the fiber length. This is due to the fact that the coefficient $\alpha(\omega)L$ increases, which leads to a decrease on the accidental coincidences, and due to the increase on the fiber input pump power with the increase of the fiber length, since we use $\gamma P_x(0) z_e = 0.25$. Results also show that for fiber lengths $L > 800$ m, the scenario where we consider fiber loss and Raman scattering is almost equal to the one where $f_R = 0$ and $\alpha(\omega) = 0$.

In optical fibers, the spontaneous FWM process can be used to create polarization entangled states through a fiber loop [53]. The fiber loop give rises to two co-polarized FWM processes, one clockwise (CW) and other counterclockwise (CCW), creating a polarization entangled Bell state of $|\Phi^{\pm}\rangle = (|H\rangle_s|H\rangle_i \pm |V\rangle_s|V\rangle_i)/\sqrt{2}$, where H and V denote horizontal and vertical linear polarizations, respectively [17], [53]. The degree of quantum entanglement can be tested with the CHSH form of the Bell's inequality [51]. The violation of CHSH inequality in optical fibers using spontaneous FWM

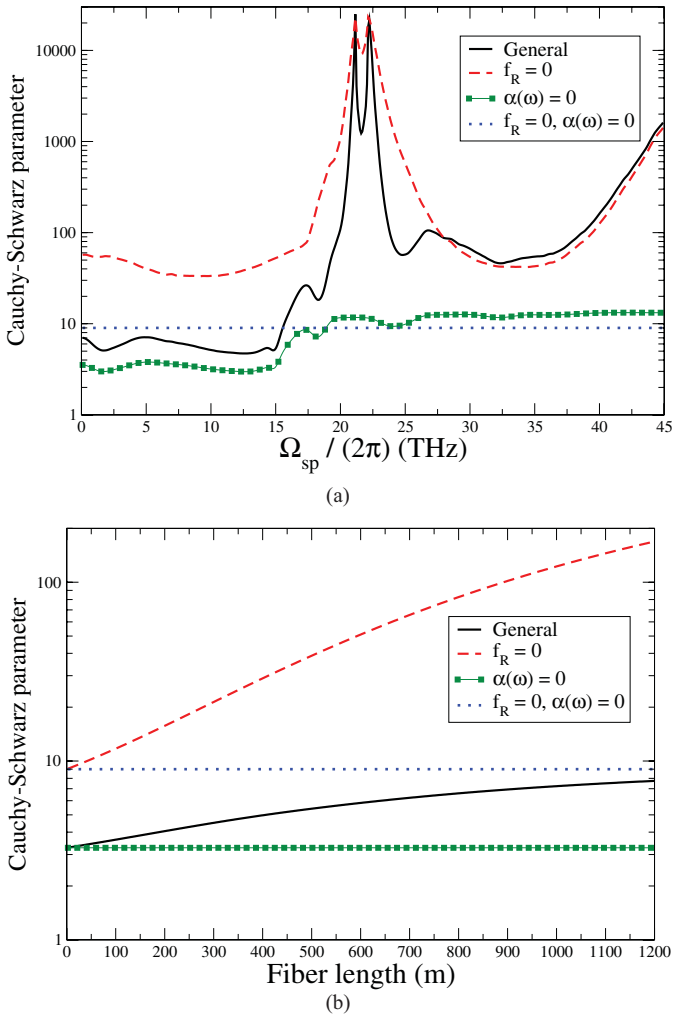

Fig. 2. Cauchy–Schwarz correlation parameter, $\mathcal{G}^{CS}(0)$. (a) Given by (28) as a function of frequency detuning. (b) Given as a function of fiber length. In plot (b) $\Omega_{sp}/(2\pi) = 3$ (THz). The fiber parameters used are equal to the ones used in Fig. 1.

process has been reported in several experimental works [11], [17]–[20], [54]. According with [6], the CHSH parameter $\mathcal{S}(\tau)$ is given by

$$\mathcal{S}(\tau) = 2\sqrt{2}\, V(\tau) \leq 2, \tag{34}$$

where $V(\tau)$ is the fringe pattern visibility, given by

$$V(\tau) = \frac{G^{(2)}_{(si)}(\tau) - \mathcal{I}_i(L,t)\mathcal{I}_s(L,t+\tau)}{G^{(2)}_{(si)}(\tau) + \mathcal{I}_i(L,t)\mathcal{I}_s(L,t+\tau)}, \tag{35}$$

where $\mathcal{I}_u$ and $G^{(2)}_{(si)}$ are given by (21) and (29), respectively. A violation of the CHSH inequality happens when $\mathcal{S}(\tau) > 2$.

Figure 3 shows the CHSH parameter, $\mathcal{S}(0)$, given by (34) as a function of frequency detuning, Fig. 3(a), and as a function of fiber input pump power, Fig. 3(b). In Fig. 3(c) we present the fringe pattern visibility associated to the CHSH parameter, given by (35), as a function of the time delay between signal and idler waves, for five different values of frequency detuning between pump and signal fields. Results present in Fig. 3(a) show that, in general the fiber loss has a positive impact on

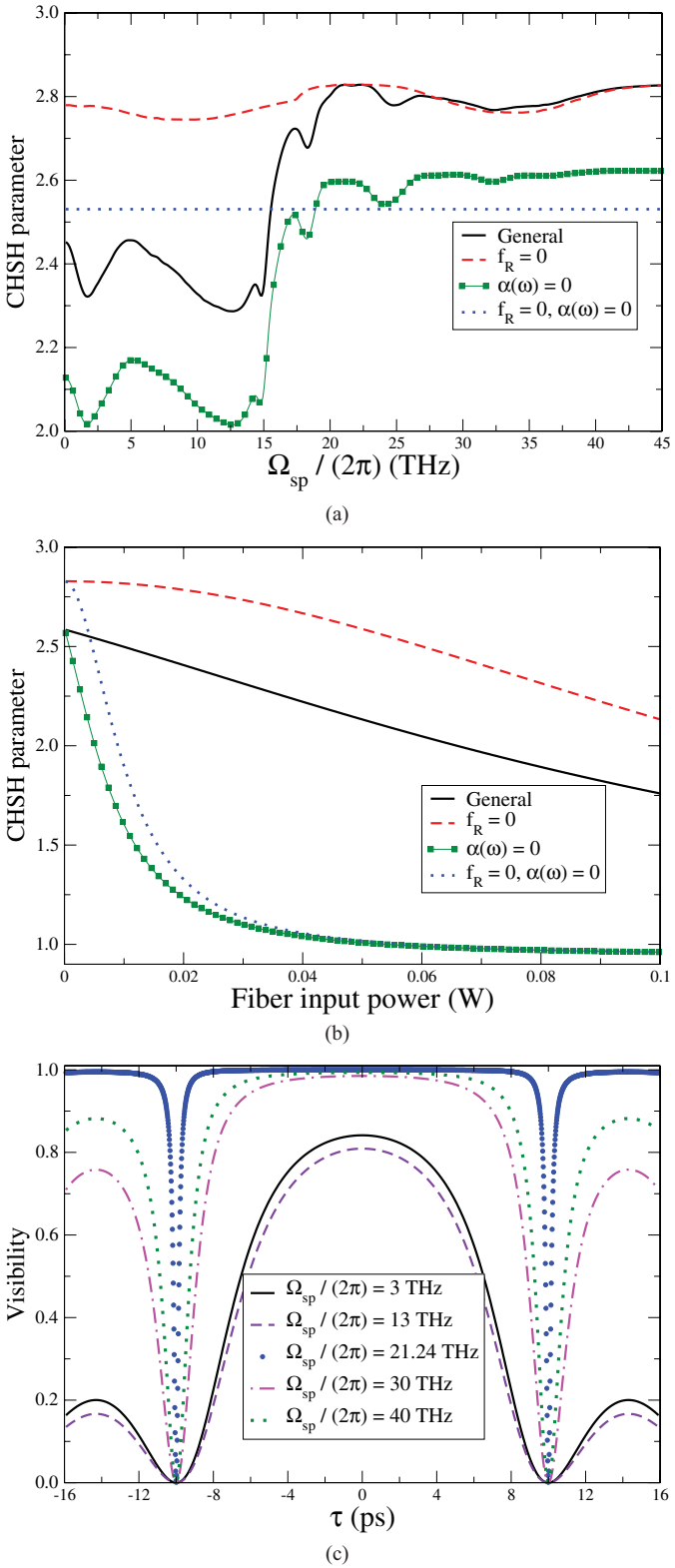

Fig. 3. CHSH parameter, $\mathcal{S}(0)$. (a) Given by (34) as a function of frequency detuning. (b) Given as a function of fiber input pump power. In plot (b) $\Omega_{sp}/(2\pi) = 3$ (THz). (c) Visibility, $V(\tau)$, given by (35) as a function of time delay between signal-idler photon pairs. In (c), the signal and idler optical filters are assumed to have a bandwidth of $\Delta\nu = 100$ GHz. The fiber parameters used are equal to the ones used in Fig. 1.

the degree of quantum entanglement, since the value of $\mathcal{S}(0)$ parameter increase in the presence of loss. In particularly, in the range 20-45 (THz) $\mathcal{S}(0)$ is close to the maximum value of

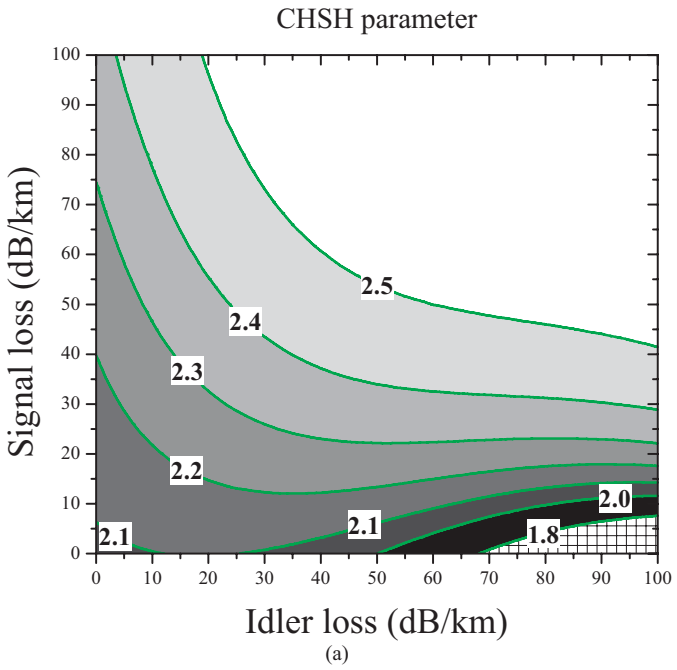

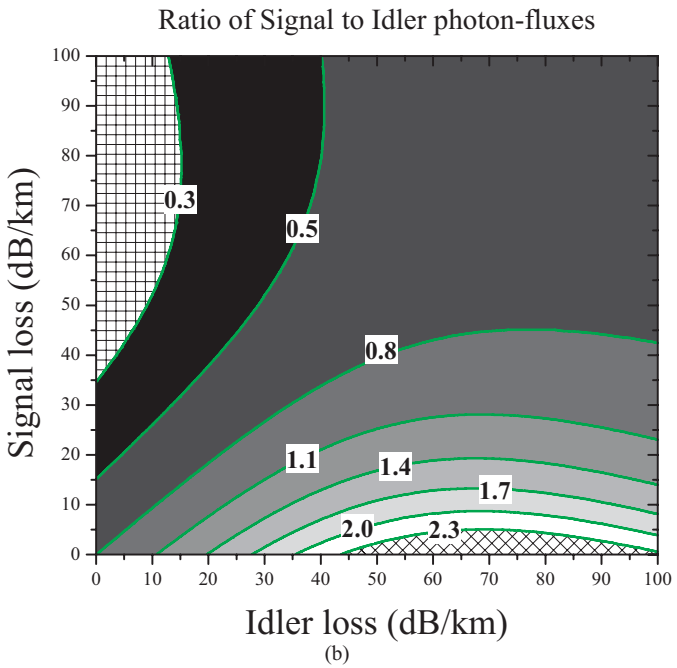

Fig. 4. (a) Contour plot for the CHSH parameter, $\mathcal{S}(0)$, given by (34) as a function of idler loss, $\alpha_{\tilde{i}}$, and as a function of signal loss, $\alpha_{\tilde{s}}$. (b) Contour plot for the ratio $\mathcal{I}_s(L,0)/\mathcal{I}_i(L,0)$, given by (22) as a function of $\alpha_{\tilde{i}}$ and $\alpha_{\tilde{s}}$. In the figure, we use $\Omega_{sp}/(2\pi) = 3$ (THz). The fiber parameters used are equal to the ones used in Fig. 1.

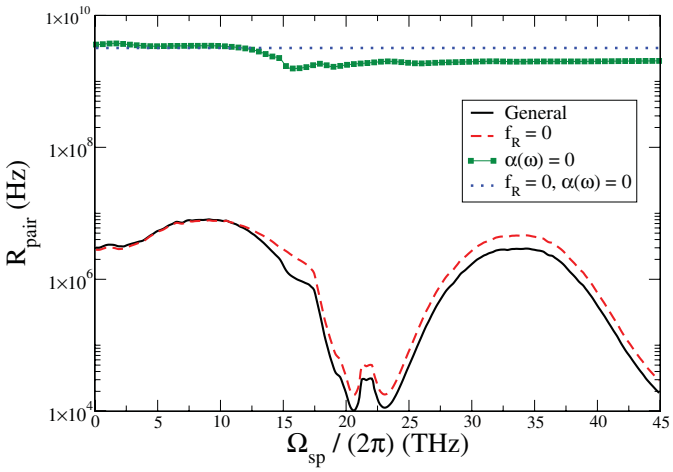

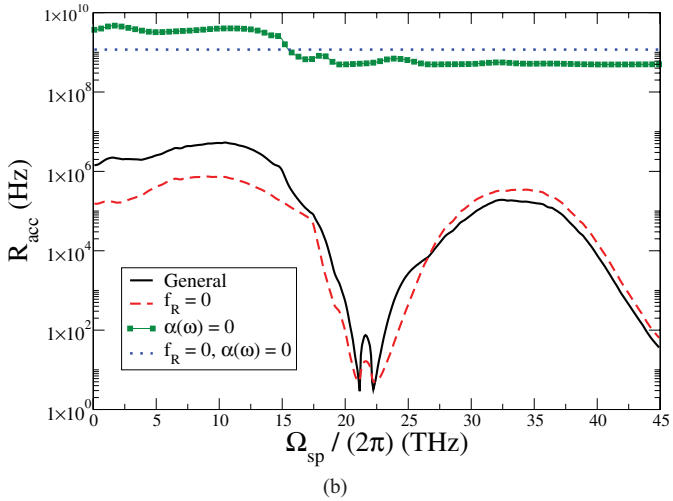

Fig. 5. (a) True plot and (b) accidental plot of coincidences counting rates given by (33a) and (33b), respectively, as a function of frequency detuning between pump and signal fields. In both plots, we have used $\Delta\nu = 100$ GHz, and $\tau_c = 30$ ps. The fiber parameters used are equal to the ones used in Fig. 1.

$2\sqrt{2}$, even considering both fiber loss and Raman scattering. For $\Omega_{sp}/(2\pi) < 20$ (THz) the Raman scattering process reduces the value of $\mathcal{S}(0)$.

Results present in Fig 3(b) show that an increase on the fiber input pump power completely degrades the degree of quantum entanglement. This is due to an increase on the probability of multiphoton generation, since an increase on the pump power leads to an increase in the stimulated FWM and Raman scattering processes [6]. In that scenario, the individual signal and idler photon-fluxes are dominant over the signal-idler photon pairs.

Results present in Fig. 3(c) show that $V(\tau)$ is close to 1 for $\Omega_{sp}/(2\pi) \approx 21$ (THz), which correspond to the maximum on the spectrum of the fiber loss presented on Fig. 1(c). For $\Omega_{sp}/(2\pi) < 21$ (THz), the visibility decreases due to the presence of uncorrelated Raman scattered photons. Due to that fact, the minimum on the visibility is for $\Omega_{sp}/(2\pi) \approx 13$ (THz), the peak of Raman gain, see Fig. 1(d). For $\Omega_{sp}/(2\pi) > 21$ (THz), we obtain again $V(0) \approx 1$, because in that frequency range $\alpha(\omega)L \gg 1$.

Figure 4 shows the contour plot for the $\mathcal{S}(0)$ parameter, Fig. 4(a), and for the ratio of signal to idler photon-fluxes $\mathcal{I}_s(L,0)/\mathcal{I}_i(L,0)$, Fig. 4(b), as a function of idler, $\alpha_{\tilde{i}}$, and signal, $\alpha_{\tilde{s}}$, fiber loss coefficients. It can be seen in Fig. 4(a) that, a strong violation of the CHSH inequality is obtained for high values of both signal and idler loss coefficients. Results also show that, if the signal loss is almost negligible and the idler loss is very high it is not observed a violation of the CHSH inequality. This is due to the fact that, the ratio

of signal to idler photon fluxes, $\mathcal{I}_s(L,0)/\mathcal{I}_i(L,0)$, is much higher than one, see Fig 4(b). Otherwise, when the signal loss coefficient is high and the idler loss is almost null, we observe a violation of the CHSH inequality, according with the result present in Fig. 4(a). In that case, $\mathcal{I}_s(L,0)/\mathcal{I}_i(L,0)$ is less than one, as can be seen in Fig. 4(b). From Fig. 4(a) and Fig. 4(b), we can see that a maximum on $\mathcal{S}(0)$ value happens when $\mathcal{I}_s(L,0)/\mathcal{I}_i(L,0)$ lies between 0.5 and 0.8, with $\alpha_{\bar{s}} > 45$ dB/km.

Figure 5 shows the true, Fig. 5(a), and accidental, Fig. 5(b), coincidences counting rates given by (33a) and (33b), respectively, as a function of frequency detuning between pump and signal. It can be seen in Fig. 5 that the fiber loss decreases significantly the photon counting rate. However, that decrease is more pronounced on the rate of accidental coincidence counts, Fig. 5(b). Assuming a lossless medium the maximum true-to-accidental ratio (TAR) is around 4 ($R_{\text{pair}} \approx 2$ GHz and $R_{\text{acc}} \approx 0.5$ GHz). When the loss is considered the maximum value for the TAR is approximately 8000 ($R_{\text{pair}} \approx 23$ kHz and $R_{\text{acc}} \approx 3$ Hz), see Fig. 5(a) and Fig. 5(b), and see also Fig. 1(c). In this case most of generated photons are signal-idler pairs generated through spontaneous FWM. For $\Omega_{sp}/(2\pi) < 20$ (THz) the Raman scattering process is the main source of uncorrelated photons, which leads to a higher increase on R_{acc} than on R_{pair}. According with the results present in Fig. 5, photon pairs generated through FWM in the regime $\alpha(\omega)L \gg 1$ are suitable to be used in sources of entangled photon pairs for quantum key distribution systems, since the expected TAR value can go up to 8000, which is much higher than the values in waveguides with $\alpha(\omega)L \ll 1$, typical measured values are of the order of 10 [4], [11], [15].

VI. Conclusion

In summary, we investigate the impact of fiber loss on the generation of quantum-correlated photon pairs through the spontaneous FWM process. We show that the presence of fiber loss and an absorption reservoir does not change the statistics of the individual signal and idler fields. The frequency dependence of the fiber loss coefficient completely changes the obtained spectrum of the photon-flux at fiber output, since the signal (idler) photon-flux depends on the idler (signal) loss coefficient. Our analysis also show that, the fiber loss increase the expected signal-idler correlation at fiber output, due to the fact that the accidental coincidences from the individual signal and idler fields decreases. This impact of the fiber loss is verified through the analysis of the CHSH parameter. In that case, the presence of loss increases the value of $\mathcal{S}(0)$ parameter, when compared with the case $\alpha(\omega) = 0$. However, our results show that the Raman scattering process remains the main source of uncorrelated photon pairs, over the frequency range 0-20 (THz). In that frequency range, the fiber loss have a positive impact on the violation of the CHSH parameter. The fiber loss increases the purity of the photon pair correlation, due to the fact that fiber absorption reduces the rate of uncorrelated photons generated by Raman scattering inside the fiber. Finally, we have shown that to maximize the $\mathcal{S}(0)$ parameter the ratio $\mathcal{I}_s(L,0)/\mathcal{I}_i(L,0) < 0.8$. In addition, we have shown that waveguides with non-negligible loss, $\alpha(\omega)L \gg 1$ can be used for efficient generation of quantum-correlated photon pairs. In that case, we can use waveguides with length $L \gg 1/\alpha(\omega)$ which allow to use a regime of low pump power, increasing the quality of the photon pairs.

Acknowledgment

The authors would like to thank NKT Photonics for the experimental value of the loss spectrum for the NL-PM-750 fiber.

References

[1] N. Gisin, G. Ribordy, W. Tittel, and H. Zbinden, "Quantum cryptography," *Rev. Mod. Phys.*, vol. 74, no. 1, pp. 145–195, 2002.

[2] D. de Brito and R. Ramos, "Analysis of heralded single-photon source using four-wave mixing in optical fibers via Wigner function and its use in quantum key distribution," *IEEE J. Quantum Electron.*, vol. 46, no. 5, pp. 721–727, May 2010.

[3] C. Liang, K. F. Lee, J. Chen, and P. Kumar, "Distribution of fiber-generated polarization entangled photon-pairs over 100 km of standard fiber in OC-192 WDM environment," in *Proc. Opt. Fiber Commun. Conf. Expo. Nat. Fiber Opt. Eng. Conf.*, 2006, pp. 1–3.

[4] P. Kumar, "Practical quantum communication and cryptography for WDM optical networks," in *Proc. AIP Conf. Quantum Commun. Meas. Comput.*, 2004, pp. 3–11.

[5] G. Agrawal, *Nonlinear Fiber Optics*, 3rd ed. New York: Academic, 2001.

[6] Q. Lin, F. Yaman, and G. P. Agrawal, "Photon-pair generation in optical fibers through four-wave mixing: Role of Raman scattering and pump polarization," *Phys. Rev. A*, vol. 75, no. 2, pp. 023803-1–023803-20, 2007.

[7] N. A. Silva, N. J. Muga, and A. N. Pinto, "Effective nonlinear parameter measurement using FWM in optical fibers in a low power regime," *IEEE J. Quantum Electron.*, vol. 46, no. 3, pp. 285–291, Mar. 2010.

[8] X. Gai, R. P. Wang, C. Xiong, M. J. Steel, B. J. Eggleton, and B. Luther-Davies, "Near-zero anomalous dispersion $Ge_{11.5}As_{24}Se_{64.5}$ glass nanowires for correlated photon pair generation: Design and analysis," *Opt. Express*, vol. 20, no. 2, pp. 776–786, Jan. 2012.

[9] *NL-PM-750 Data Sheet*. (2009) [Online]. Available: http://www.nktphotonics.com/files/files/NL-PM-750-090612.pdf

[10] C. Xiong, L. G. Helt, A. C. Judge, G. D. Marshall, M. J. Steel, J. E. Sipe, and B. J. Eggleton, "Quantum-correlated photon pair generation in chalcogenide As_2S_3 waveguides," *Opt. Express*, vol. 18, no. 15, pp. 16206–16216, Jul. 2010.

[11] J. Fan, A. Migdall, J. Chen, and E. Goldschmidt, "Microstructure-fiber-based source of photonic entanglement," *IEEE J. Sel. Topics Quantum Electron.*, vol. 15, no. 6, pp. 1724–1732, Nov.–Dec. 2009.

[12] A. Politi, M. J. Cryan, J. G. Rarity, S. Yu, and J. L. O'Brien, "Silica-on-silicon waveguide quantum circuits," *Science*, vol. 320, no. 5876, pp. 646–649, 2008.

[13] M. Fiorentino, P. Voss, J. Sharping, and P. Kumar, "All-fiber photon-pair source for quantum communications," *IEEE Photon. Technol. Lett.*, vol. 14, no. 7, pp. 983–985, Jul. 2002.

[14] J. E. Sharping, M. Fiorentino, and P. Kumar, "Observation of twin-beam-type quantum correlation in optical fiber," *Opt. Lett.*, vol. 26, no. 6, pp. 367–369, Mar. 2001.

[15] J. Fan, A. Dogariu, and L. J. Wang, "Generation of correlated photon pairs in a microstructure fiber," *Opt. Lett.*, vol. 30, no. 12, pp. 1530–1532, Jun. 2005.

[16] J. Chen, K. F. Lee, C. Liang, and P. Kumar, "Fiber-based telecom-band degenerate-frequency source of entangled photon pairs," *Opt. Lett.*, vol. 31, no. 18, pp. 2798–2800, Sep. 2006.

[17] H. Takesue and K. Inoue, "Generation of polarization-entangled photon pairs and violation of Bell's inequality using spontaneous four-wave mixing in a fiber loop," *Phys. Rev. A*, vol. 70, no. 3, pp. 031802-1–031802-4, 2004.

[18] X. Li, P. L. Voss, J. E. Sharping, and P. Kumar, "Optical-fiber source of polarization-entangled photons in the 1550 nm telecom band," *Phys. Rev. Lett.*, vol. 94, no. 5, pp. 053601-1–053601-4, Feb. 2005.

[19] X. Li, C. Liang, K. F. Lee, J. Chen, P. L. Voss, and P. Kumar, "Integrable optical-fiber source of polarization-entangled photon pairs in the telecom band," *Phys. Rev. A*, vol. 73, no. 5, pp. 052301-1–052301-6, May 2006.

[20] J. Fan, M. D. Eisaman, and A. Migdall, "Bright phase-stable broadband fiber-based source of polarization-entangled photon pairs," *Phys. Rev. A*, vol. 76, pp. 043836-1–043836-4, Oct. 2007.
[21] H. Takesue and K. Inoue, "Generation of 1.5-μm band time-bin entanglement using spontaneous fiber four-wave mixing and planar light-wave circuit interferometers," *Phys. Rev. A*, vol. 72, no. 4, pp. 041804-1–041804-4, Oct. 2005.
[22] H. Takesue, "Long-distance distribution of time-bin entanglement generated in a cooled fiber," *Opt. Express*, vol. 14, no. 8, pp. 3453–3460, Apr. 2006.
[23] X. Li, L. Yang, X. Ma, L. Cui, Z. Y. Ou, and D. Yu, "All-fiber source of frequency-entangled photon pairs," *Phys. Rev. A*, vol. 79, no. 3, pp. 033817-1–033817-9, Mar. 2009.
[24] C. Xiong, G. D. Marshall, A. Peruzzo, M. Lobino, A. S. Clark, D.-Y. Choi, S. J. Madden, C. M. Natarajan, M. G. Tanner, R. H. Hadfield, S. N. Dorenbos, T. Zijlstra, V. Zwiller, M. G. Thompson, J. G. Rarity, M. J. Steel, B. Luther-Davies, B. J. Eggleton, and J. L. O'Brien, "Generation of correlated photon pairs in a chalcogenide As_2S_3 waveguide," *Appl. Phys. Lett.*, vol. 98, no. 5, pp. 051101-1–051101-3, 2011.
[25] L. J. Wang, C. K. Hong, and S. R. Friberg, "Generation of correlated photons via four-wave mixing in optical fibres," *J. Opt. B, Quantum Semiclassical Opt.*, vol. 3, no. 5, pp. 346–352, 2001.
[26] J. Chen, X. Li, and P. Kumar, "Two-photon-state generation via four-wave mixing in optical fibers," *Phys. Rev. A*, vol. 72, no. 3, pp. 033801-1–033801-3, Sep. 2005.
[27] O. Alibart, J. Fulconis, G. K. L. Wong, S. G. Murdoch, W. J. Wadsworth, and J. G. Rarity, "Photon pair generation using four-wave mixing in a microstructured fibre: Theory versus experiment," *New J. Phys.*, vol. 8, no. 5, pp. 1–67, 2006.
[28] P. L. Voss and P. Kumar, "Raman-effect induced noise limits on $\chi^{(3)}$ parametric amplifiers and wavelength converters," *J. Opt. B, Quantum Semiclassical Opt.*, vol. 6, no. 8, pp. S762–S770, 2004.
[29] P. L. Voss and P. Kumar, "Raman-noise-induced noise-figure limit for $\chi^{(3)}$ parametric amplifiers," *Opt. Lett.*, vol. 29, no. 5, pp. 445–447, Mar. 2004.
[30] P. L. Voss, K. G. Köprülü, and P. Kumar, "Raman-noise-induced quantum limits for $\chi^{(3)}$ nondegenerate phase-sensitive amplification and quadrature squeezing," *J. Opt. Soc. Amer. B*, vol. 23, no. 4, pp. 598–610, 2006.
[31] Q. Lin, F. Yaman, and G. P. Agrawal, "Photon-pair generation by four-wave mixing in optical fibers," *Opt. Lett.*, vol. 31, no. 9, pp. 1286–1288, May 2006.
[32] Q. Lin and G. P. Agrawal, "Silicon waveguides for creating quantum-correlated photon pairs," *Opt. Lett.*, vol. 31, no. 21, pp. 3140–3142, Nov. 2006.
[33] P. D. Drummond and J. F. Corney, "Quantum noise in optical fibers. I. Stochastic equations," *J. Opt. Soc. Amer. B*, vol. 18, no. 2, pp. 139–152, 2001.
[34] P. D. Drummond, *Coherence and Quantum Optics VII*. New York: Springer-Verlag, 1996, pp. 323–332.
[35] L. Boivin, F. X. Kärtner, and H. A. Haus, "Analytical solution to the quantum field theory of self-phase modulation with a finite response time," *Phys. Rev. Lett.*, vol. 73, no. 2, pp. 240–243, 1994.
[36] F. X. Kärtner, D. J. Dougherty, H. A. Haus, and E. P. Ippen, "Raman noise and soliton squeezing," *J. Opt. Soc. Amer. B*, vol. 11, no. 7, pp. 1267–1276, 1994.
[37] R. W. Boyd, *Nonlinear Optics*, 2nd ed. New York: Academic, 2003.
[38] Q. Lin and G. P. Agrawal, "Effects of polarization-mode dispersion on fiber-based parametric amplification and wavelength conversion," *Opt. Lett.*, vol. 29, no. 10, pp. 1114–1116, May 2004.
[39] R. W. Hellwarth, *Third-Order Optical Susceptibilities of Liquids and Solids*. New York: Pergamon, 1977.
[40] N. Silva, N. Muga, and A. Pinto, "Influence of the stimulated Raman scattering on the four-wave mixing process in birefringent fibers," *J. Lightw. Technol.*, vol. 27, no. 22, pp. 4979–4988, Nov. 2009.
[41] N. A. Silva, N. J. Muga, and A. N. Pinto, "Evolution of first-order sidebands from multiple FWM processes in HiBi optical fibers," *Opt. Commun.*, vol. 284, no. 13, pp. 3408–3415, Jun. 2011.
[42] D. Hollenbeck and C. D. Cantrell, "Multiple-vibrational-mode model for fiber-optic raman gain spectrum and response function," *J. Opt. Soc. Amer. B*, vol. 19, no. 12, pp. 2886–2892, 2002.
[43] Q. Lin and G. P. Agrawal, "Raman response function for silica fibers," *Opt. Lett.*, vol. 31, no. 21, pp. 3086–3088, 2006.
[44] M. Artoni and R. Loudon, "Propagation of nonclassical light through an absorbing and dispersive slab," *Phys. Rev. A*, vol. 59, no. 3, pp. 2279–2290, 1999.
[45] A. Zonnenberg, "Supercontinuum generation in the picosecond regime," Ph.D. thesis, Leiden Inst. Physics, Leiden Univ., Leiden, The Netherlands, Sep. 2006.
[46] N. A. Silva, A. J. Almeida, and A. N. Pinto, "Interference in a quantum channel due to classical four-wave mixing in optical fibers," *IEEE J. Quantum Electron.*, vol. 48, no. 4, pp. 472–479, Apr. 2012.
[47] R. Loudon, *The Quantum Theory of Light*, 3rd ed. New York: Oxford Univ. Press, 2000.
[48] E. A. Goldschmidt, M. D. Eisaman, J. Fan, S. V. Polyakov, and A. Migdall, "Spectrally bright and broad fiber-based heralded single-photon source," *Phys. Rev. A*, vol. 78, no. 1, pp. 013844-1–013844-4, Jul. 2008.
[49] P. L. Voss, R. Tang, and P. Kumar, "Measurement of the photon statistics and the noise figure of a fiber-optic parametric amplifier," *Opt. Lett.*, vol. 28, no. 7, pp. 549–551, Apr. 2003.
[50] J. F. Clauser, "Experimental distinction between the quantum and classical field-theoretic predictions for the photoelectric effect," *Phys. Rev. D*, vol. 9, no. 4, pp. 853–860, 1974.
[51] J. F. Clauser, M. A. Horne, A. Shimony, and R. A. Holt, "Proposed experiment to test local hidden-variable theories," *Phys. Rev. Lett.*, vol. 23, pp. 880–884, Oct. 1969.
[52] M. Kozierowski, "Violation of the Cauchy–Schwarz inequality and anticorrelation effect in second-harmonic generation," *Phys. Rev. A*, vol. 36, no. 6, pp. 2973–2975, 1987.
[53] J. Chen, J. B. Altepeter, and P. Kumar, "Quantum-state engineering using nonlinear optical sagnac loops," *New J. Phys.*, vol. 10, no. 12, pp. 123019-1–123019-19, 2008.
[54] A. Almeida, S. Carneiro, N. Silva, N. Muga, and A. Pinto, "Polarization-entangled photon pairs using spontaneous four-wave mixing in a fiber loop," in *Proc. IEEE EUROCON Int. Conf. Comput. Tool*, Apr. 2011, pp. 1–4.

Nuno A. Silva was born in Fafe, Portugal, in 1981. He received the Degree in physics from the University of Minho, Braga, Portugal, and the M.S. degree in physics from the University of Aveiro, Aveiro, Portugal, in 2006 and 2008, respectively. He is currently pursuing the Ph.D. degree with the University of Aveiro.

He joined the Institute of Telecommunications, Aveiro, in 2007, where he is currently a Researcher with the Optics Communications Group. His current research interests include nonlinear fiber optics, polarization, and quantum effects in optical fibers.

Armando Nolasco Pinto (M'99–SM'07) received the Degree in electronic and telecommunications engineering and the Ph.D. degree in electrical engineering from the University of Aveiro, Aveiro, Portugal, in 1994 and 1999, respectively.

He became an Assistant Professor with the Electrical, Telecommunications and Informatics Department, University of Aveiro, in 2000, and a Researcher with the Institute of Telecommunications. He was a Visiting Professor with the Institute of Optics, University of Rochester, Rochester, NY, from 2006 to 2007. He currently leads a research group with the Institute of Telecommunications focusing on high-speed optical communication systems and networks. He has authored or co-authored more than 100 scientific papers in international journals and conferences.

Dr. Pinto is a member of the Optical Society of America. He served in the technical committee of various scientific international conferences. He is currently an Editorial Board Member of the *International Journal of Optics*.